

Hybrid vector beams with non-uniform orbital angular momentum density induced by designed azimuthal polarization gradient

Lei Han(韩磊), Shuxia Qi(齐淑霞), Sheng Liu(刘圣), Peng Li(李鹏), Huachao Cheng(程华超), Jianlin Zhao(赵建林)

Citation: Chin. Phys. B . 2020, 29(9): 094203 . **doi:** 10.1088/1674-1056/aba09d
Journal homepage: http://cpb.iphy.ac.cn; http://iopscience.iop.org/cpb

What follows is a list of articles you may be interested in

Pulse shaping of bright-dark vector soliton pair

Yan Zhou(周延), Yuefeng Li(李月锋), Xia Li(李夏), Meisong Liao(廖梅松), Jingshan Hou(侯京山), Yongzheng Fang(房永征)

Chin. Phys. B . 2020, 29(5): 054202 . **doi:** 10.1088/1674-1056/ab7b56

Multiple trapping using a focused hybrid vector beam

Li Zhang(张莉), Xiaodong Qiu(邱晓东), Lingwei Zeng(曾令伟), Lixiang Chen(陈理想)

Chin. Phys. B . 2019, 28(9): 094202 . **doi:** 10.1088/1674-1056/ab33ef

Simultaneous polarization separation and switching for 100-Gbps DP-QPSK signals in backbone networks

Yu-Long Su(苏玉龙), Huan Feng(冯欢), Hui Hu(胡辉), Wei Wang(汪伟), Tao Duan(段弢), Yi-Shan Wang(王屹山), Jin-Hai Si(司金海), Xiao-Ping Xie(谢小平), He-Ning Yang(杨合宁), Xin-Ning Huang(黄新宁)

Chin. Phys. B . 2019, 28(2): 024216 . **doi:** 10.1088/1674-1056/28/2/024216

Polarization-based range-gated imaging in birefringent medium:Effect of size parameter

Heng Tian(田恒), Jing-Ping Zhu(朱京平), Shu-Wen Tan(谭树文), Jing-Jing Tian(田晶晶), Yun-Yao Zhang(张云尧), Xun Hou(侯洵)

Chin. Phys. B . 2018, 27(12): 124203 . **doi:** 10.1088/1674-1056/27/12/124203

β-BaB_2O_4 with special cut-angle applied to single crystal cascaded third-harmonic generation

Hong-Kai Ren(任宏凯), Hong-Wei Qi(亓宏伟), Zheng-Ping Wang(王正平), Zhi-Xin Wu(吴志心), Meng-Xia Wang(王梦霞), Yu-Xiang Sun(孙玉祥), Xun Sun(孙洵), Xin-Guang Xu(许心光)

Chin. Phys. B . 2018, 27(11): 114202 . **doi:** 10.1088/1674-1056/27/11/114202

SPECIAL TOPIC — Optical field manipulation

Hybrid vector beams with non-uniform orbital angular momentum density induced by designed azimuthal polarization gradient*

Lei Han(韩磊), Shuxia Qi(齐淑霞), Sheng Liu(刘圣)†, Peng Li(李鹏), Huachao Cheng(程华超), and Jianlin Zhao(赵建林)‡

MOE Key Laboratory of Material Physics and Chemistry under Extraordinary Conditions, and Shaanxi Key Laboratory of Optical Information Technology, School of Physical Science and Technology, Northwestern Polytechnical University, Xi'an 710129, *China*

(Received 17 May 2020; revised manuscript received 20 June 2020; accepted manuscript online 29 June 2020)

Based on angular amplitude modulation of orthogonal base vectors in common-path interference method, we propose an interesting type of hybrid vector beams with unprecedented azimuthal polarization gradient and demonstrate in experiment. Geometrically, the configured azimuthal polarization gradient is indicated by intriguing mapping tracks of angular polarization states on Poincaré sphere, more than just conventional circles for previously reported vector beams. Moreover, via tailoring relevant parameters, more special polarization mapping tracks can be handily achieved. More noteworthily, the designed azimuthal polarization gradients are found to be able to induce azimuthally non-uniform orbital angular momentum density, while generally uniform for circle-track cases, immersing in homogenous intensity background whatever base states are. These peculiar features may open alternative routes for new optical effects and applications.

Keywords: hybrid vector beam, polarization gradient, polarization mapping track, orbital angular momentum density

PACS: 42.25.Ja, 42.60.Jf, 42.50.Tx, 42.40.Jv **DOI:** 10.1088/1674-1056/aba09d

1. Introduction

Recent decades, vector beams have witnessed exponential increasement of research interests on itself.[1,2] Owing to peculiar spatially variant polarization structures, vector beams present many extraordinary optical properties, especially in tight-focusing aspect, such as optical needle and optical chain,[3–5] *etc*.[6,7] These stunning optical properties provide great potential value in various application fields, including super-resolution microscopy,[8] optical data storage and encryption,[9] and laser fabrication,[10] *etc*.[11–14] Driven by these outstanding features, constructing distinctive polarization structure has become one of topic issues.[15–17] Up to now, diverse types of vector beams have been reported, for instance, cylindrical vector beams,[18] vector beams with multiple polarization singularities,[19] and hybrid vector beams,[20–23] *etc*.[24–26]

Hybrid vector beams are one significant and fascinating type of vector beams.[20–22] By superposition of a pair of orthogonal linear polarization basis vectors carrying spiral phase, Wang *et al*. proposed one kind of hybrid vector beams for the first time.[20] Replacing linear polarization basis states with more general elliptically polarized basis vectors, *Xu et al*. further produced arbitrary vector fields with hybrid polarization state.[21] In addition, Gilad generated hybrid polarized beams by transmitting radially polarized light through a wave plate,[22] and so on. Compared with linearly polarized vector beams, besides peculiar tight focusing properties, hybrid vector beams may possess other especial features. Remarkably, azimuthally varying polarized vector beams have recently been demonstrated on its possibility of carrying orbital angular momentum (OAM) related to Pancharatnam phase.[27–31] Conceivably, for azimuthally varying polarized vector beams, diverse azimuthal polarization gradients may give birth to various optical properties. Hence, constructing special azimuthal polarization variation is meaningful for exploring new optical phenomena and effects. Geometrically, azimuthal polarization gradient can be intuitively indicated by projection track of angular polarization states on Poincaré sphere.[31] Although various azimuthally varying polarized vector beams have been produced, up to now, most of reported cases present circular tracks on Poincaré sphere.[29–31]

As is well known, via the common-path interference method, vector beams can be generated by superposition of a pair of orthonormal polarization components carrying predesigned spatial phase structures.[32,33] That is, the electric

*Project supported by the National Key Research and Development Program of China (Grant No. 2017YFA0303800), the National Natural Science Foundation of China (Grant Nos. 11634010, 61675168, 91850118, 11774289, and 11804277), the Fundamental Research Funds for the Central Universities, China (Grant No. 3102019JC008), and the Basic Research Plan of Natural Science in Shaanxi Province, China (Grant Nos. 2018JM1057 and 2019JM-583).

†Corresponding author. E-mail: shengliu@nwpu.edu.cn

‡Corresponding author. E-mail: jlzhao@nwpu.edu.cn

© 2020 Chinese Physical Society and IOP Publishing Ltd

field distribution can be expressed as follows:

$$\begin{aligned}\boldsymbol{E} &= u(r,\varphi)\left[\alpha_0 \mathrm{e}^{\mathrm{i}\delta_\alpha}\boldsymbol{e}_\alpha + \beta_0 \mathrm{e}^{\mathrm{i}\delta_\beta}\boldsymbol{e}_\beta\right] \\ &= u(r,\varphi)\exp\left(\mathrm{i}\frac{\delta_\alpha+\delta_\beta}{2}\right) \\ &\quad\times\left[\alpha_0\exp\left(\mathrm{i}\frac{\delta_\alpha-\delta_\beta}{2}\right)\boldsymbol{e}_\alpha\right. \\ &\quad\left.+\beta_0\exp\left(-\mathrm{i}\frac{\delta_\alpha-\delta_\beta}{2}\right)\boldsymbol{e}_\beta\right], \end{aligned} \tag{1}$$

where (r,φ) is the polar coordinate, $u(r,\varphi)$ represents the holistic complex amplitude being independent on polarization structures, $\boldsymbol{e}_\alpha$ and $\boldsymbol{e}_\beta$ are a pair of orthogonal basis vectors, α_0 and β_0 denote the relative amplitude profiles of these two basis vectors with $|\alpha_0|^2+|\beta_0|^2=1$, and δ_α and δ_β are additional phase distributions attached by $\boldsymbol{e}_\alpha$ and $\boldsymbol{e}_\beta$, respectively. From Eq. (1), we can know that for a preconcerted pair of basis vectors, tailoring relative amplitude and phase distributions at distinct spatial positions will give birth to diverse polarization structures. However, until now, most of reported vector beams focus on engineering relative phase distribution within spatially uniform relative amplitude profiles, *i.e.*, the ratio of α_0 and β_0 being same over entire beam cross section.

In this paper, by unlocking relative amplitude modulation along azimuthal coordinate, we design an intriguing kind of hybrid vector beams with unprecedented azimuthal polarization gradient, *i.e.*, non-circle mapping track, and demonstrate few cases in experiment. The tailoring behavior of modulation parameters on polarization gradient is explored in detail. More strikingly, the designed angular polarization gradients are found to be able to induce azimuthally non-uniform OAM density within homogeneous intensity background regardless of what base states are, while generally uniform OAM density for vector beams exhibiting circular mapping tracks.

The rest of the paper is organized as follows. In Section 2, we introduce the proposed scheme and discuss in detail the tailoring behavior of modulation parameters on polarization gradient. In Section 3, we further study the orbital angular momentum induced by peculiar polarization gradient. In Section 4, we demonstrate the generation of few hybrid vector beams in experiment. Finally, we conclude the paper in Section 5.

2. Theoretical description

The azimuthal amplitude modulation we propose here is described as

$$\alpha_0(r,\varphi)=\cos(l\varphi+\varphi_0), \quad \beta_0(r,\varphi)=\sin(l\varphi+\varphi_0), \tag{2}$$

where l is coined as amplitude modulation factor and φ_0 is initial phase with $\varphi_0\in[0,\pi]$. Considering the independence of polarization structure on $\delta_\alpha+\delta_\beta$, hereinafter, only the cases with $\delta_\alpha=-\delta_\beta=m\varphi$ are discussed without losing generality. Therefore, we now get the electric field as

$$\begin{aligned}\boldsymbol{E} &= u(r,\varphi)\left[\cos(l\varphi+\varphi_0)\mathrm{e}^{\mathrm{i}m\varphi}\boldsymbol{e}_\alpha\right. \\ &\quad\left.+\sin(l\varphi+\varphi_0)\mathrm{e}^{-\mathrm{i}m\varphi}\boldsymbol{e}_\beta\right]. \end{aligned} \tag{3}$$

As seen in Eq. (3), for any pair of basis vectors $(\boldsymbol{e}_\alpha, \boldsymbol{e}_\beta)$, the synthetic polarization structure is determined by parameters (l,m,φ_0). Obviously, according to whether l and m are zero, we can classify synthetic beams into the following four categories.

(i) For cases of $l=0$ and $m=0$, the electric field will correspondingly become $\boldsymbol{E}=u(r,\varphi)[\cos\varphi_0\boldsymbol{e}_\alpha+\sin\varphi_0\boldsymbol{e}_\beta]$. It can be clearly known that the generated light beams are scalar beams for arbitrary basis vectors $(\boldsymbol{e}_\alpha, \boldsymbol{e}_\beta)$. And the exact polarization state is determined by the value of φ_0.

(ii) For cases of $l=0$ while $m\neq 0$, if the initial angle $\varphi_0=0$, $\pi/2$ or π, only one base state has non-zero complex amplitude, hence, the resulting beam is a scalar beam carrying spiral phase. While for cases with $\varphi_0\neq 0$, $\pi/2$, and π, conventional azimuthally varying polarized vector beams are achieved as presented in Refs. [29–31]. In other words, the previously reported cases can actually be viewed as special cases of our general description. For these vector beams, the polarization mapping tracks on Poincaré sphere display circular shape. The plane of circular track is perpendicular to the connection line of the base vectors. And the central position and diameter of circles are dependent on base vectors and φ_0.[30]

To illustrate and manifest corresponding properties of vector beams intuitively, we present one case of $(0,-1,\pi/4)$ in Fig. 1(a). Without losing generality, here we take circularly polarized base vectors as representative, *i.e.*, $(\boldsymbol{e}_\alpha, \boldsymbol{e}_\beta)=(\boldsymbol{e}_\mathrm{R}, \boldsymbol{e}_\mathrm{L})$. As shown, the right- and left-hand polarized components have the same intensity profile, while opposite for spiral phase maps. Hence, the generated beam is the well-known radial vector beam. The synthetic polarization structure is depicted in the third column, where red and blue ellipses represent right- and left-handed elliptical polarization ellipses for $s_3\geq 0$ and $s_3\leq 0$, respectively. In calculations, we set the global amplitude $u(r,\varphi)$ as the 1st order Bessel Gaussian profile, *i.e.*, $u(r,\varphi)=\exp(-r^2/w_0^2)\mathrm{J}_1(2r/w_0)$, where $w_0=9$ mm is the beam waist. Moreover, the evolution curve of normalized Stokes parameters is plotted in the fourth column to show polarization variation along the angular direction. Further, we draw the polarization mapping track on the Poincaré sphere in pink color in the fifth column. Meanwhile, we also present the mapping track of another case $(0,-1,\pi/6)$ in cyan color. Visually, as mentioned above, various values of φ_0 give different radiuses. And both circle planes are perpendicular to the linking line of the right- and left-handed circular polarization states.

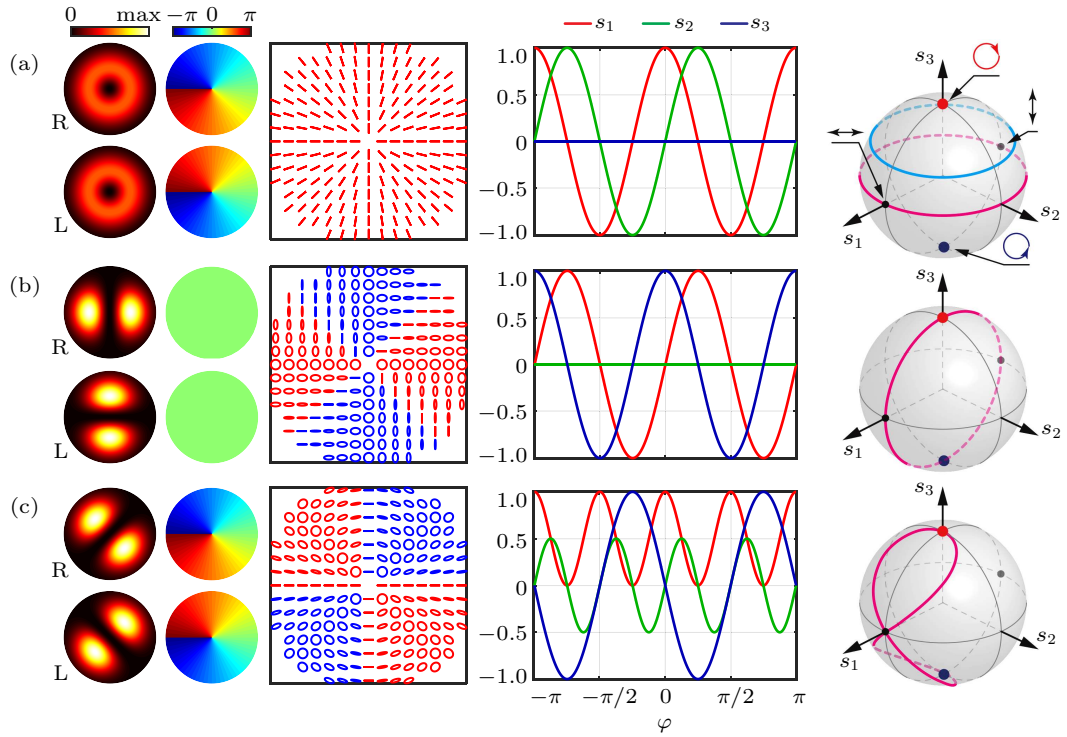


Fig. 1. Illustration of the proposed scheme under circularly polarized basis vector. The cases (0, −1, $\pi/4$), (1, 0, 0), and (1, 1, $\pi/4$) are presented in panels (a)–(c) in turn. The first and second columns display the intensity and phase profiles of right-(R) and left-handed (L) circular polarization states, respectively. The synthetic polarization, normalized Stokes parameters along angular direction and polarization mapping tracks on Poincaré sphere are depicted in the third to the fifth columns, respectively. The red and blue ellipses represent right- and left-handed polarization states, respectively.

(iii) For $l \neq 0$ while $m = 0$, the electric field is $\boldsymbol{E} = u(r,\varphi)[\cos(l\varphi+\varphi_0)\boldsymbol{e}_\alpha + \sin(l\varphi+\varphi_0)\boldsymbol{e}_\beta]$. Therefore, the synthetic light beams are also azimuthally varying polarized vector beams. Geometrically, the polarization mapping tracks on Poincaré sphere are always meridian circles. However, distinct to the cases in case (ii), the circular track will travel through the two base vectors. As seen from case $(1,0,0)$ depicted in Fig. 1(b), a non-zero l gives non-uniform relative amplitude ratio of two orthogonal components. Thus, a hybrid vector beam having meridian mapping circle is constructed.

(iv) More noteworthily, when both l and m are non-zero, *i.e.*, $l \neq 0$ and $m \neq 0$, an unusual kind of vector beams will be constructed, which is the most intriguing core of the proposed scheme. As a representative, we give the case $(1, -1, \pi/4)$ in Fig. 1(c). Obviously, significantly different from circle projection tracks in Figs. 1(a) and 1(b), there is a distinctive mapping track seem like an infinity symbol in Fig. 1(c). The special mapping tracks indicate straightly that the proposed scheme can enable different polarization states on Poincaré sphere to establish unprecedented connection, thus possess capability to configurate intriguing azimuthal polarization gradient.

To reveal the modulation effect of l and m on azimuthal polarization gradient, in Figs. 2(a)–2(h), we further depict some cases with different l and m. As is well known, besides Stokes parameters, any polarization state can be briefly described by a set of angle coordinates $(2\psi, 2\chi)$ on Poincaré sphere.[21,29] Here, 2ψ and 2χ stand for longitude and latitude angles of polarization state, respectively. In the second row of Fig. 2, we plot the varying curves of longitude and latitude along azimuthal coordinate. According to the relationship of Stokes parameters and longitude and latitude angles, we can get the corresponding result as follows:

$$\tan 2\psi = -\tan(2m\varphi), \quad \sin 2\chi = \cos(2l\varphi + 2\varphi_0). \tag{4}$$

Comparing the results in Fig. 2(a) with Fig. 2(f) and in Fig. 2(b) with Fig. 2(h), and together with more other cases, it is found that for different sets of (l, m) with same ratio of l/m, the polarization mapping tracks will share same shape. And various ratios will give rise to diverse interesting shaped tracks. Furthermore, via analyzing variation of longitude and latitude angles along angular coordinate, we find that for certain ratio of l/m, the specific values of l and m decide the polarization variation period along azimuthal coordinate, as displayed in Figs. 2(a) and 2(f) as well as Figs. 2(b) and 2(h). Moreover, we can get the fact that l determines the gradient of latitude, and m together with l controls the gradient of longitude. Here, it should be noted that though the tangent value of longitude angle is only determined by m, owing to periodical feature of tangent function, the longitude angle will have distinct varying curve associated with l, such as seen in Figs. 2(a) and 2(e). In addition, comparing the result in Fig. 1(c) with that in Fig. 2(a), it is found that φ_0 plays a role of controlling position of mapping track on Poincaré sphere. All above-mentioned features can be verified by more other cases.

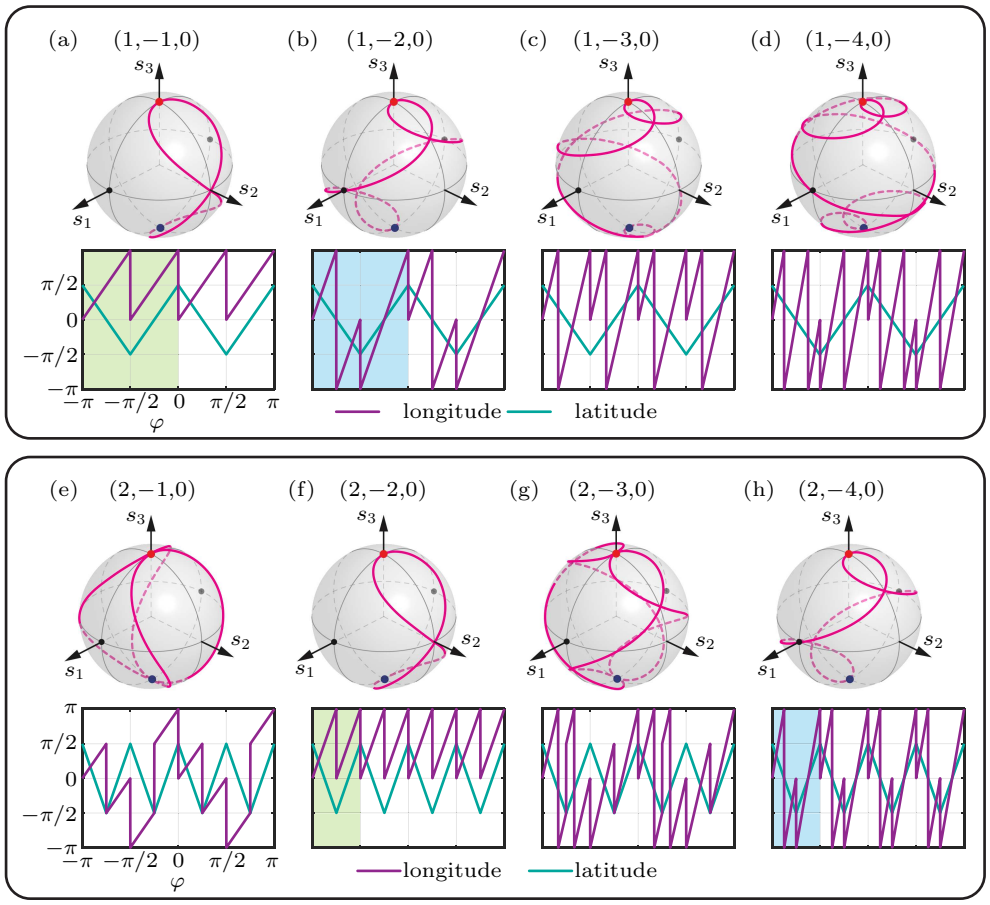


Fig. 2. Modulation effect of l and m on polarization gradient. The polarization structures, the polarization mapping tracks, and the evolution curves of longitude and latitude angles along angular direction are depicted in the first to the third rows, respectively.

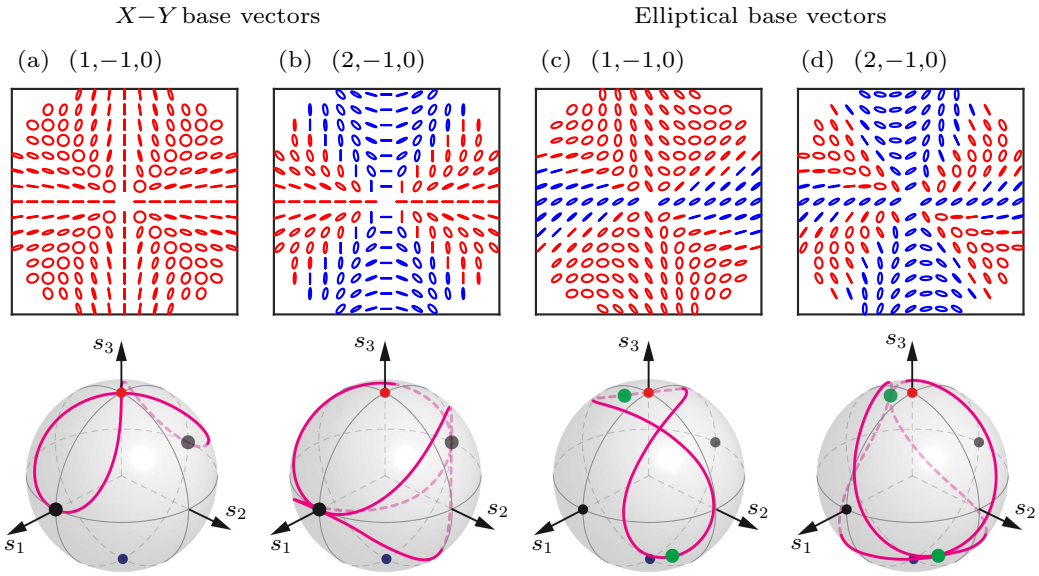


Fig. 3. Hybrid vector beams under various base states. The red and blue ellipses represent right- and left-handed polarization states, respectively.

In fact, the aforementioned tailoring behavior of l and m on polarization gradient applies to any orthogonal base vectors. As shown in Fig. 3, it can be clearly seen that under different base vectors, when hybrid vector beams have same l/m, the polarization mapping tracks will share same shape. And the position of mapping track on Poincaré sphere depends on the base vectors. Moreover, if we set arbitrary $\boldsymbol{e}_\alpha$ and $\boldsymbol{e}_\beta$ as north and south poles respectively, the modulation feature of l and m on latitude and longitude angles is same as that under circularly polarized base vectors. In Figs. 3(c) and 3(d), the green points on Poincaré sphere stand for the chosen elliptical polarized base states, and their longitude and latitude angles

$(2\psi,\ 2\chi)$ are $(\pi/3,\ -\pi/6)$ and $(-2\pi/3,\ \pi/6)$, respectively. According to the longitude and latitude angles $(2\psi,\ 2\chi)$, the corresponding polarization states can be described based on X–Y basis vectors as follows:

$$\begin{aligned}&\boldsymbol{E}(2\psi,2\chi)\\ =&\ \frac{1}{\sqrt{2}}\left[\sin(\chi+\pi/4)\,\mathrm{e}^{-\mathrm{i}\psi}+\cos(\chi+\pi/4)\,\mathrm{e}^{\mathrm{i}\psi}\right]\boldsymbol{e}_x\\ &+\mathrm{i}\frac{1}{\sqrt{2}}\left[\sin(\chi+\pi/4)\,\mathrm{e}^{-\mathrm{i}\psi}-\cos(\chi+\pi/4)\,\mathrm{e}^{\mathrm{i}\psi}\right]\boldsymbol{e}_y. \quad (5)\end{aligned}$$

3. Non-uniform OAM density associated with azimuthal polarization gradient

By analyzing OAM density of hybrid vector beams with $l\neq0$ and $m\neq0$ in theory, we excitingly find that the proposed azimuthal polarization gradient can induce fancy non-uniform OAM density. As presented in Ref. [31], for azimuthally varying polarized vector beams, regardless of $\boldsymbol{e}_\alpha$ and $\boldsymbol{e}_\beta$, the z component of OAM density comprises two parts associated with azimuthal gradient,

$$l_z=(\boldsymbol{r}\times\boldsymbol{p}_\perp^o)_z\propto u^2\frac{\partial\Phi}{\partial\varphi}+u^2\,\mathrm{Im}\left[\alpha^*\frac{\partial\alpha}{\partial\varphi}+\beta^*\frac{\partial\beta}{\partial\varphi}\right], \quad (6)$$

where Φ represents the phase distribution and is corresponding to $(\delta_\alpha+\delta_\beta)/2$ in our discussed cases. Besides, there is

$$\alpha=\cos(l\varphi+\varphi_0)\,\mathrm{e}^{\mathrm{i}m\varphi},\quad \beta=\sin(l\varphi+\varphi_0)\,\mathrm{e}^{-\mathrm{i}m\varphi}. \quad (7)$$

As shown in Eq. (6), the first term is induced by phase gradient like conventional scalar vortex phase. In contrast, the second term in Eq. (6) is associated with the polarization gradient in the angular direction. By substituting Eq. (7) into Eq. (6), we can obtain the polarization-gradient-related OAM density as follows:

$$l_{z2}\propto 2m\cos(2l\varphi+2\varphi_0)\,u^2. \quad (8)$$

Remarkably, for azimuthally uniform amplitude distribution, *i.e.*, $u(r,\varphi)=u(r)$, the polarization-gradient-related OAM density is closely relevant to $(l,\ m,\ \varphi_0)$. Obviously, for the cases with $l=0$, the OAM density profile is spatially uniform, while for the cases with $l\neq0$, the OAM density features variation along the azimuthal coordinate φ_0. Thus, a non-zero l together with a non-zero m will give rise to the non-uniform OAM density. And m plays a role on controlling the maximum amplitude of the local OAM density. Additionally, as seen from Eq. (8), the non-uniform OAM density has cosine distribution along the azimuthal coordinate, thus for the cases with $l\neq0$ and $m\neq0$, the integral of the OAM density over beam cross section is always zero, *e.g.*, the total OAM is zero. That is, we can achieve azimuthally variant OAM density under homogeneous intensity background, which is in fact rare for conventional scalar and vector beams with azimuthally varying polarization states as reported previously.[29–31] Moreover, holding the same intensity background, diverse OAM density distributions can be achieved via tailoring aforementioned modulation parameters.

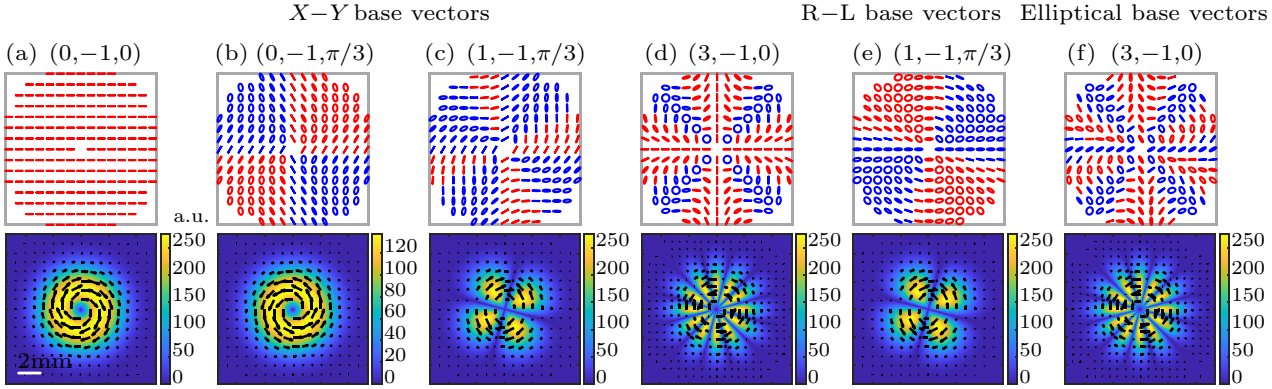


Fig. 4. Polarization structures (upper) and transverse Poynting vector patterns (lower) of hybrid vector beams with (a)–(d): $(0,-1,0)$, $(0,-1,\pi/3)$, $(1,1,\pi/3)$, and $(3,-1,0)$ under X–Y base vectors, (e): $(1,1,\pi/3)$ under R–L base vectors, and (f): $(3,-1,0)$ a pair of elliptical base vectors. The red and blue ellipses represent right- and left-handed polarization states, respectively.

For illustration and considering the proportional relation of linear momentum density with Poynting vector, in Fig. 4, we show the transverse part of Poynting vector, *i.e.*, transverse energy flux density distribution, of a few cases under X–Y, R–L, and a pair of elliptical base vectors. Here, the longitude and latitude angles of the orthogonal elliptical base vectors are $(\pi/3,\ -\pi/6)$ and $(-2\pi/3,\ \pi/6)$, respectively. The Poynting vector distribution can indirectly reflect the polarization-gradient-related OAM density. As we can see, in Fig. 4(a), owing to $l=0$ and $\varphi_0=0$, the vector beam degenerates into an x-polarized scalar beam, therefore, the azimuthally uniform transverse Poynting vector totally originates from spiral phase, where black arrows indicate the direction. For the case with $\varphi_0=\pi/3$, a hybrid vector beam with circular mapping track is constructed as shown in Fig. 4(b). Hence, the transverse Poynting vector is induced by azimuthally varying po-

larization structures and keeps cylindrical symmetry. Nevertheless, notably, the maximum value becomes lower than that in Fig. 4(a), which is in consistent with the result in Ref. [31]. In contrast to Figs. 4(a) and 4(b), in agreement with predictions according to Eq. (8), a non-zero $l = 1$ in Fig. 4(c) and $l = 3$ in Fig. 4(d) induces periodically inhomogeneous transverse Poynting vector along azimuthal direction. And as expected, the variation period can be manipulated via adjusting l. Moreover, comparing Fig. 4(c) with Fig. 4(e) and Fig. 4(d) with Fig. 4(f), it is obviously seen that for same parameters, though polarization structures are different under distinct base vectors, the induced OAM density distributions have the same patterns, which is consistent with our prediction. The unique azimuthally inhomogeneous OAM density may draw different phenomena in optical force and manipulation.

4. Experiment setup and results

To realize the proposed hybrid vector beams in experiment, it is crucial to steer the relative amplitude profiles of two orthogonal constituents. Considering this condition, we employ the efficient experimental setup proposed by Liu *et al.*,[34] as shown in Fig. 5. For detailed description on principle, please refer to Section 2 in Ref. [34]. Note, in our experiment, a half-wave plate (HWP3) and a quarter-wave plate (QWP) are needed to transform the synthetic light beam into aimed vector beam. To this end, the angles between x direction and fast axes of HWP3 and QWP need to be adjusted properly in order to alter p and s components into arbitrary prescribed basis vectors. The produced polarization structures are measured via a polarization measuring system (PMS) proposed in Ref. [35]. Using the encoding technique pioneered in Ref. [36], both amplitude and phase information for any l, m, and φ_0 can be conveniently encoded onto one phase map displayed in SLM.

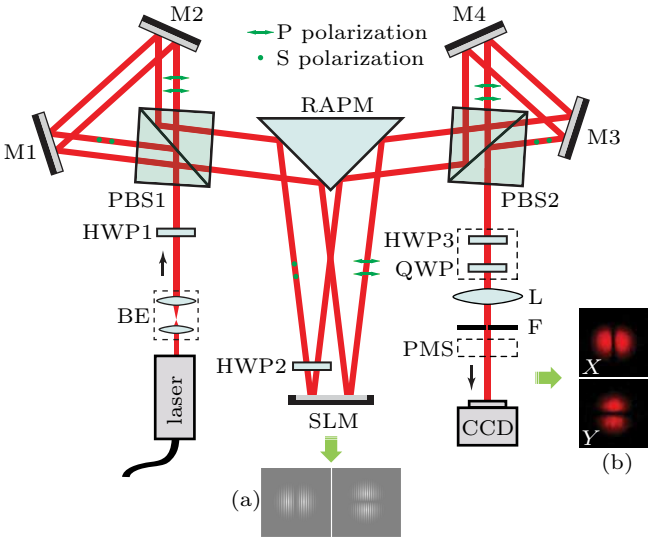


Fig. 5. Experimental setup. BE: beam expansion module; HWP: half-wave plate; PBS: polarizing beam splitter; M1–M4: mirrors; RAPM: right-angle prism mirror; SLM: spatial light modulator; QWP: quarter-wave plate; L: lens; F: spatial filter; PMS: polarization measuring system; CCD: charge coupled device. Insets: (a) the computer-generated holograms and (b) the measured intensity patterns of x and y components for the case $(1,0,0)$ on the base of X–Y basis vectors, *i.e.*, radial vector beam.

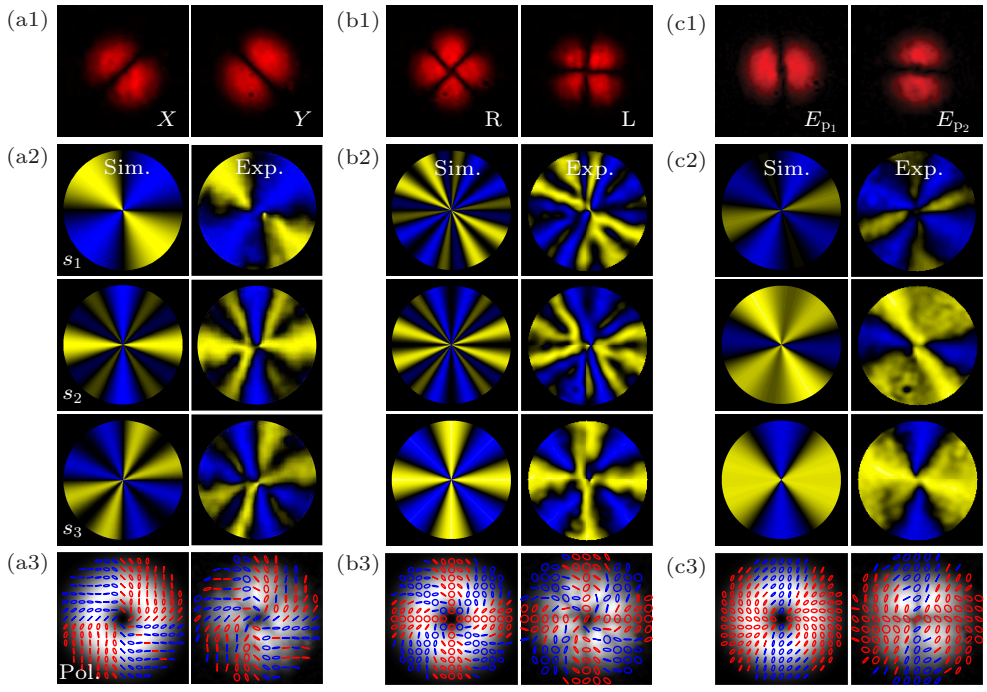


Fig. 6. Experimental and theoretical results for (a) $(1, -2, \pi/4)$ under X–Y basis vector, (b) $(2, -3, 0)$ under R–L basis vector, and (c) $(1, -1, 0)$ under elliptical basis vector E_{p_1}–E_{p_2}. The longitude and latitude of E_{p_1} and E_{p_2} on Poincaré sphere are $(-\pi/3, \pi/3)$ and $(2\pi/3, -\pi/3)$, respectively. The measured intensity patterns of orthogonal basis vectors are shown in panels (a1)–(c1). Theoretical (left) and experimental (right) results of Stokes parameters and produced polarization structures are depicted in panels (a2)–(c2) and (a3)–(c3) in turn. The red and blue ellipses represent right- and left-handed polarization states, respectively.

Figures 6(a)–6(c) exhibit the theoretical and experimental results of three representative cases under X–Y, R–L, and a pair of elliptical basis vectors E_{p_1}–E_{p_2}, respectively. The longitude and latitude of the chosen elliptical basis vectors E_{p_1}–E_{p_2} on Poincaré sphere are $(-\pi/3,\ \pi/3)$ and $(2\pi/3,\ -\pi/3)$, respectively. The corresponding modulation parameters for each case are in turn $(1,-2,\pi/4)$, $(2,-3,0)$, and $(1,-1,0)$. As shown in the figure, evidently, the generated polarization structure as well as measured Stokes parameters are in good agreement with the theoretical results, which provides a proof of feasibility of the proposed scheme. The differences between experimental and theoretical results, including the intensity patterns and polarization structures, may owe to many factors, including quality of laser beam, imaging quality of CCD, and post-processing program, *etc*.

5. Conclusions

In conclusion, based on angular amplitude modulation of orthogonal base states, we propose and demonstrate an unusual type of hybrid vector beams with intriguing azimuthal polarization gradient. Geometrically, the synthetic polarization structures here present unprecedented non-circle mapping tracks on Poincaré sphere. Moreover, the polarization gradient, *i.e*., polarization mapping tracks on Poincaré sphere, can be simply and flexibly manipulated via arranging relevant modulation parameters. More interestingly, the produced peculiar azimuthal polarization gradient is found to able to induce azimuthal non-uniform OAM density within homogenous intensity background, while in general uniform for circle-tracks cases. These features may provide a new way for focal fields shaping and local OAM tailoring, *etc*.

References

[1] Halina R D, Andrew F, Berry M V, Dennis M R, David L A, Masud M, Cornelia D, Christina A, Peter B, Thomas B, Ebrahim K, Lorenzo M, Miles P, Monika R M, Natalia M L, Nicholas P B, Rosales-Guzmán C, Belmonte A, Torres J P, Tyler W N, Mark B, Reuven G, Alexander B S, Jacquiline R, Andrew G W, Robert F, Alan E W, Guodong X, Benjamin M and Andrew M W 2017 *J. Opt.* **19** 013001

[2] Zhan Q 2009 *Adv. Opt. Photon.* **1** 1

[3] Youngworth K S and Brown T G 2000 *Opt. Express* **7** 77

[4] Wang H, Shi L, Lukyanchuk B, Sheppard C and Chong C T 2008 *Nat. Photon.* **2** 501

[5] Zhao Y, Zhan Q, Zhang Y and Li Y 2005 *Opt. Lett.* **30** 848

[6] Han L, Liu S, Li P, Zhang Y, Cheng H and Zhao J 2018 *Phys. Rev. A* **97** 053802

[7] Wang S, Li X, Zhou J and Gu M 2014 *Opt. Lett.* **39** 5022

[8] Chen R, Agarwal K, Sheppard C J R and Chen X 2013 *Opt. Lett.* **38** 3111

[9] Gu M, Li X and Cao Y 2014 *Light: Sci. Appl.* **3** e177

[10] Cheng H, Li P, Liu S, Chen P, Han L, Zhang Y, Hu W and Zhao J 2017 *Appl. Phys. Lett.* **111** 141901

[11] Novotny L, Beversluis M R, Youngworth K S and Brown T G 2001 *Phys. Rev. Lett.* **86** 5251

[12] Xiao F, Shang W, Zhu W, Han L, Premaratne M, Mei T and Zhao J 2018 *Photon. Res.* **6** 157

[13] Shang W, Xiao F, Zhu W, Han L, Premaratne M, Mei T and Zhao J 2019 *Opt. Express* **27** 4944

[14] Neugebauer M, Wozniak P, Bag A, Leuchs G and Banzer P 2016 *Nat. Commun.* **7** 11286

[15] Li P, Zhang Y, Liu S, Ma C, Han L, Cheng H and Zhao J 2016 *Opt. Lett.* **41** 2205

[16] Pan Y, Gao X, Cai M, Zhang G, Li Y, Tu C and Wang H 2016 *Opt. Lett.* **41** 3161

[17] Otte E, Tekce K and Denz C 2018 *J. Opt.* **20** 105606

[18] Liu Z, Liu Y, Ke Y, Liu Y, Shu W, Luo H and Wen S 2017 *Photon. Res.* **5** 15

[19] Han L, Liu S, Li P, Zhang Y, Cheng H, Gan X and Zhao J 2016 *Appl. Opt.* **55** 9049

[20] Wang X, Li Y, Chen J, Guo C, Ding J and Wang H 2010 *Opt. Express* **18** 10786

[21] Xu D, Gu B, Rui G, Zhan Q and Cui Y 2016 *Opt. Express* **24** 4177

[22] Lerman G M, Stern L and Levy U 2010 *Opt. Express* **18** 27650

[23] Beckley A M, Brown T G and Alonso M A 2010 *Opt. Express* **18** 10777

[24] Pan Y, Li Y, Li S, Ren Z, Si Y, Tu C and Wang H 2013 *Opt. Lett.* **38** 3700

[25] Li P, Wu D, Zhang Y, Liu S, Li Y, Qi S and Zhao J 2018 *Photon. Res.* **6** 756

[26] Chang C, Gao Y, Xia J, Nie S and Ding J 2017 *Opt. Lett.* **42** 3884

[27] Yang Y, Zhao Q, Liu L, Liu Y, Rosalesguzman C and Qiu C 2019 *Phys. Rev. Appl.* **12** 064007

[28] Yang Y, Thirunavukkarasu G, Babiker M and Yuan J 2017 *Phys. Rev. Lett.* **119** 094802

[29] Zhang D, Feng X, Cui K, Liu F and Huang Y 2015 *Sci. Rep.* **5** 11982

[30] Yang C, Chen Y, Wu S and Fuh A Y 2016 *Sci. Rep.* **6** 31546

[31] Pan Y, Gao X, Ren Z, Wang X, Tu C, Li Y and Wang H 2016 *Sci. Rep.* **6** 29212

[32] Wang X, Ding J, Ni W, Guo C and Wang H 2007 *Opt. Lett.* **32** 3549

[33] Liu S, Li P, Peng T and Zhao J 2012 *Opt. Express* **20** 21715

[34] Liu S, Qi S, Zhang Y, Li P, Wu D, Han L and Zhao J 2018 *Photon. Res.* **6** 228

[35] Liu S, Han L, Li P, Zhang Y, Cheng H and Zhao J 2017 *Appl. Phys. Lett.* **110** 171112

[36] Davis J A, Cottrell D M, Campos J, Yzuel M J and I Moreno 1999 *Appl. Opt.* **38** 5004